INSTITUTE OF PHYSICS PUBLISHING JOURNAL OF PHYSICS: CONDENSED MATTER

J. Phys.: Condens. Matter **14** (2002) 4857–4879 PII: S0953-8984(02)31883-6

Computer simulation study of low-energy excitations of silicate glasses

Erika J Palin, Kostya O Trachenko and Martin T Dove

Mineral Physics Group, Department of Earth Sciences, University of Cambridge, Downing Street, Cambridge CB2 3EQ, UK

Received 13 December 2001, in final form 2 April 2002
Published 2 May 2002
Online at stacks.iop.org/JPhysCM/14/4857

Abstract

Ten silicate and aluminosilicate glasses with different number densities and connectivities were studied by molecular dynamics simulation using the computer program DL_POLY [1]. The radial distribution functions, phonon densities of states and flexibilities of the glass networks were determined, and compared with those determined for silica [2]. The large-scale flexibility of silica was found to be similar to that of some of the glasses studied in this work, particularly in relation to rigid-unit-mode-type motions. The degree of localization of vibrations in fully networked glasses was found to be similar to that in silica, but the vibrations in glasses containing non-bridging oxygen atoms were found to be more localized. This is thought to be due to clustering of alkali cations, which in turn necessarily produces clusters of tetrahedra.

(Some figures in this article are in colour only in the electronic version)

1. Introduction

The low-energy dynamics of silicate glasses has attracted a lot of interest. Part of the interest is driven by attempts to understand the origin of the so-called 'boson peak' [3], a peak seen in measurements of the inelastic spectra at around 5 meV (although this phenomenon is not discussed in this paper). Another motivation is to identify potential tunnelling states that give rise to anomalous thermodynamic properties at low temperatures.

Recently [2] we reported studies of the low-energy dynamics of silica glass based on the results of molecular dynamics simulations (MDSs) and analysis in terms of rigid-unit modes (RUMs). RUMs are normal modes of motion in which structural polyhedra, such as SiO_4 and AlO_4 tetrahedra or AlO_6 octahedra, can move without distortion. These modes are identical to the 'floppy modes' of Thorpe *et al* [4], but are specific to motions of polyhedra. The idea that RUMs can exist in crystalline materials that can be described as frameworks of structural polyhedra, such as the various phases of silica, was invoked several decades ago to explain phase transitions in materials such as quartz, and the idea that RUMs may be responsible for low-energy excitations in silica glasses has been put forward by several authors. In order to be able to quantify the application of the RUM model to crystalline materials a computational algorithm

was developed, called the 'split-atom method', that allows us to count the number of RUMs for any wavevector in a crystal. This has allowed us to explain how RUMs are responsible for structural phase transitions [5], and the RUM model has been able to encompass other phenomena such as negative thermal expansion [6,7]. The RUM model has been supported by experimental studies, particularly inelastic neutron scattering [8,9]. In [10] and [11] we applied the RUM concept to a structural model of silica glass using our split-atom method combined with MDS. The main finding was that the silica structure has the same RUM flexibility as crystalline cristobalite, and that the RUM flexibility provides the silica glass structure with the ability to support large-amplitude localized rotations of the SiO_4 tetrahedra. These may be the motions responsible for two-level tunnelling states implicated in explanations of the low-temperature thermal properties.

The fact that the silica glass framework can support RUMs is somewhat surprising when considering the analysis of constraints and degrees of freedom that usually underpins the quantitative analysis of floppy modes in a glass. The RUM flexibility should arise from an imbalance between the number of degrees of freedom, F, and the number of constraints, C. The number of degrees of freedom of any polyhedron is $F = 6$ (3 rotations + 3 translations). The number of constraints is counted by noting that there are three constraints operating at each oxygen shared by two structural polyhedra, which arise from holding the (x, y, z) position of the corner of one polyhedra at the same (x, y, z) position as the corner of the linked polyhedron. These three constraints are shared by both linked polyhedra, and with four oxygen atoms per polyhedron we have $C = 6$ for each polyhedron. Thus we have $C = F$. The Maxwell criterion is that any framework structure is only flexible if $C < F$, and the structure is rigid if $C > F$. Network structures composed of corner-linked tetrahedra are therefore, in the Maxwell sense, on the border of being under-constrained and over-constrained, and strictly should have no RUM flexibility. For crystalline materials it is possible for symmetry to reduce the number of *independent* constraints to give $C < F$ and hence to allow the structure to support a non-zero number of RUMs. This point has been demonstrated for some model calculations, and it is found that when a material undergoes a symmetry-breaking displacive phase transition there is a drastic reduction in the number of RUMs [5]. However, it is not obvious how the symmetry argument can be applied to glass structures; nevertheless, it appears that silica glass has an inherent RUM flexibility that matches that of crystalline silica.

The purpose of this paper is to extend the analysis to other framework glasses. In particular, we focus on two families of glass structures. The first is alkali aluminosilicates in which all the tetrahedra, SiO_4 and AlO_4, can be linked into a three-dimensional framework with full connectivity. These structures are denoted as Q^4. The second family of structures is the alkali disilicates, of general form $X_2Si_2O_5$, in which SiO_4 tetrahedra are linked to three others on average. These structures are denoted as Q^3. The Q^4 structures, of which silica is also an example, have $C = F$ in the Maxwell analysis. The main purpose of analysing different compositions is that each composition will have a different structure. In the series $(KAlO_2)_x \cdot (SiO_2)_{1-x}$, different compositions x will lead to changes in the structure associated with the need to accommodate the alkali cations in voids encompassed within the network of linked tetrahedra. In particular, we find that we get a range of number densities for the Q^4 structures that varies by 25%, and it is interesting to investigate whether the changes in structure and density have an effect on the RUM flexibility. The Q^3 structures have $F - C = 1.5$ per tetrahedron in a Maxwell sense, which means that the structure will have a high degree of RUM flexibility. The previous work on silica [2, 10, 11] gave a preliminary assessment of this flexibility by artificially removing SiO_4 tetrahedra, but by working with the alkali disilicates it will be possible to quantify this under more realistic conditions. We will work with a range of Q^3 structures with number densities that vary by 35%.

The approach we take is to generate structures of the glasses using MDS (specifically, the DL_POLY code), starting from a trial crystal structure. The structures of the glass phases are analysed in terms of radial distribution functions (RDFs), and the dynamics are analysed through calculations of the density of states (from the velocity autocorrelation functions) and by calculations of participation ratios for large-scale motions. The RUM flexibility of each structure is analysed using the split-atom method. The results are compared with the earlier studies on silica glass, and trends with structure are sought through trends with number density.

We find that there is very little correlation of vibrational properties with number density, as found both by MDS and RUM analysis. The major effect of density is on the degree of localization of vibrations. The disilicates have a noticeably different RUM spectrum to the other glasses, but in the MDS this difference is somewhat less obvious.

We also observe large-scale reorientational motions similar to those observed in a recent study of silica glass.

2. Methods

2.1. Simulation samples

A number of glass compositions were investigated. Some of these contain only Si as the tetrahedral atom, whilst others contain both Si and Al. In addition, different alkali cations are present, to investigate the possible effects of changing alkali cation size on the vibrational properties of the glasses.

The simulation cell used in this work is that used by other workers [12]; a $3 \times 3 \times 3$ array of unit cells of β-cristobalite (space group $Fd\bar{3}m$, $a = 7.74$ Å, Si at (000), O at $(\frac{1}{8}\frac{1}{8}\frac{1}{8})$), where the tetrahedral and octahedral interstices are filled with the number of extra cations needed to produce the desired composition. The exact location of the extra cations within the structure is relatively unimportant, since the atoms are expected to mix on heating; however, before performing any MDS runs, the stuffed structures were relaxed using the lattice energy program GULP [13] to ensure that none was energetically unfavourable.

The glass compositions investigated were

(i) alkali disilicates $X_2Si_2O_5$, where X = Na, K, Rb,
(ii) two mixed alkali disilicates $NaKSi_2O_5$ and $NaRbSi_2O_5$,
(iii) nepheline-type compounds $XAlSiO_4$, where X = Na, K, Rb, and
(iv) compounds of the series $(KAlO_2)_x \cdot (SiO_2)_{1-x}$, of which $KAlSiO_4$ (also a member of the previous group of compounds) is the $x = \frac{1}{2}$ case. The other two compounds studied were the $x = \frac{1}{4}$ case, $KAlSi_3O_8$ (orthoclase composition), and the $x = \frac{3}{4}$ case, $K_3Al_3SiO_8$. The latter composition is not known in crystalline form, but is especially rich in potassium, and hence is suitable for investigation.

As we have noted earlier, the primary objective of our study is to compare the dynamic properties of networks with different network topologies that arise from the different densities of the different chemical compositions. In order to meet this objective, the primary requirement is for a wide range of equilibrated samples that do indeed have different densities, and which have been equilibrated with sufficient care [14, 15] to minimize the number of defects (such as silicon atoms in non-tetrahedral coordination). Where we can compare our simulated structures with experiment (see below), we find reasonable agreement. It is important to appreciate that for our objectives it is far more important to generate a wide range of different structures rather than to focus on the specific details of individual simulations. Because of the high computational demands of this objective, we did not explore issues of system size, nor did we

repeat all simulations several times to test for reproducibility (although in our initial cases we did run several simulations on the same samples in order to test our methodology). We hope that it can be appreciated that issues of ergodicity are tangential to our objective of studying the role of network density on dynamic properties.

2.2. Interatomic potential models

The interatomic potentials used in the GULP runs are given as follows. The symbol E represents energy, r an interatomic distance and θ an angle between two interatomic vectors. A zero subscript indicates an equilibrium value.

Short-range interactions were modelled by the Buckingham potential:

$$E = A\exp(-r/\rho) - \frac{C}{r^6}. \tag{1}$$

Coulomb interactions were handled via the standard Ewald sum. The oxygen atoms were modelled by the shell model where they are considered to consist of a core comprising the nucleus and inner electrons, and a massless shell of the outer electrons. The core is assigned a charge of $0.848\,19e$ and the shell a charge of $-2.848\,19e$, such that the overall charge is the formal value for the oxygen ion. The core and shell are held together by a harmonic interaction of the form

$$E = \tfrac{1}{2}k_2d^2 \tag{2}$$

where d is the core–shell separation.

Interactions of the form O–Si–O and O–Al–O were modelled by the three-body potential:

$$E = \tfrac{1}{2}K(\theta - \theta_0)^2. \tag{3}$$

2.3. Molecular dynamics simulations

In this investigation we used the DL_POLY code on a parallel computer. We were primarily interested in simulating the dynamic properties of the glasses at a certain temperature and pressure. The first stage of our method was to equilibrate the system at the relevant temperature and pressure using the NPT ensemble, allowing the size of the unit cell to relax, but not its shape. For the second stage, we switched to the NVE ensemble, for effective simulation of the atomic dynamics of the system.

For each material, the coordinates of the atoms in the simulation cell were taken, along with the interatomic potentials acting upon the relevant atoms present (see table 1), and were used in an initial DL_POLY run at a high temperature. The form of the Buckingham potential was identical to that in equation (1) but a different type of three-body potential, the screened harmonic potential, was used. This is given by

$$E = \tfrac{1}{2}K(\theta - \theta_0)^2\exp[-(r/\rho_1 + r/\rho_2)] \tag{4}$$

and was used so that the three-body terms have a smooth cutoff in space.

Formal charges were used for each ion, and Coulomb interactions were handled using the Ewald sum. All ions were treated as rigid.

The initial temperature was ideally 6000 K, as this had been used successfully by other workers [12], but for certain glasses a lower initial temperature was required to prevent the material from vaporizing. Where this was the case, the initial temperature was still kept as high as possible to ensure good mixing of the cations. The NPT ensemble was used, with a timestep of 0.002 ps, and 10 000 simulation steps (a total simulation time of 20 ps).

Table 1. Interatomic potential parameters.

Potential type	Species	Parameters			Source
Buckingham		A	ρ	C	
	Na–O	1 226.8	0.3065	0	[12]
	K–O	929.32	0.362	0	[12]
	Rb–O	2 565.507	0.3260	0	[16]
	Si–O	1 036.96	0.3259	0	[12]
	Al–O	1 460.3	0.29912	0	[17]
	O–O	3116 130	0.1515	61.39	[12]
		K	θ_0	ρ_1 $(=\rho_2)$	
Screened harmonic	O–Si–O	880.67	109.47	0.3259	[12]
(three-body)	O–Al–O[a]	880.67	109.47	0.3259	
Core–shell[b]			k_2		
	O–O		74.92		[17]

[a] Assumed identical to O–Si–O.
[b] Core–shell potential employed in GULP only.

Upon completion of the 6000 K run, the final cell parameters and atomic coordinates were used as the start configuration for another run at 5000 K, with the same ensemble, timestep and number of simulation steps. This procedure was used repeatedly to lower the temperature to 1000 K in steps of 1000 K, and then finally to 293 K. The final stage of the simulation process was to take the output from the 293 K run and perform a final run again at 293 K but with 100 000 steps and using the NVE ensemble. We determined the vibrational properties from the output from this run.

3. Analysis of structures

Due to the large numbers of data generated in this work, we have not included results for each property for all ten glasses. Instead, representative examples of structures, graphical data etc are given, and the full results are available for viewing and downloading on the internet at http://www.esc.cam.ac.uk/minsci/downloads/glass/.

3.1. Equilibrium configurations from MDS

For each glass, the structure was computed at each of the simulation temperatures. Examples of the final glass structures at 293 K are given in figure 1.

3.2. Connectivities

The theoretical connectivities of the glasses depend on the proportion of alkali cations present, since these are well documented as network modifiers. The presence of Al is also an important factor due to the difference in charge between Al and Si. It can be shown that for the disilicate compositions, the ideal average connectivity is 100% Q^3, and that all the other compositions investigated are ideally 100% Q^4 on average. A detailed explanation of this is given in [18].

To investigate the connectivity, the percentage of tetrahedral and non-tetrahedral coordination polyhedra for each glass at each temperature was determined using an in-house customization of the crystal structure program MSI Cerius^2.

At high temperatures at the beginning of the simulation, the glass structures are considerably disordered and the Al and Si atoms have a variety of coordination numbers. On

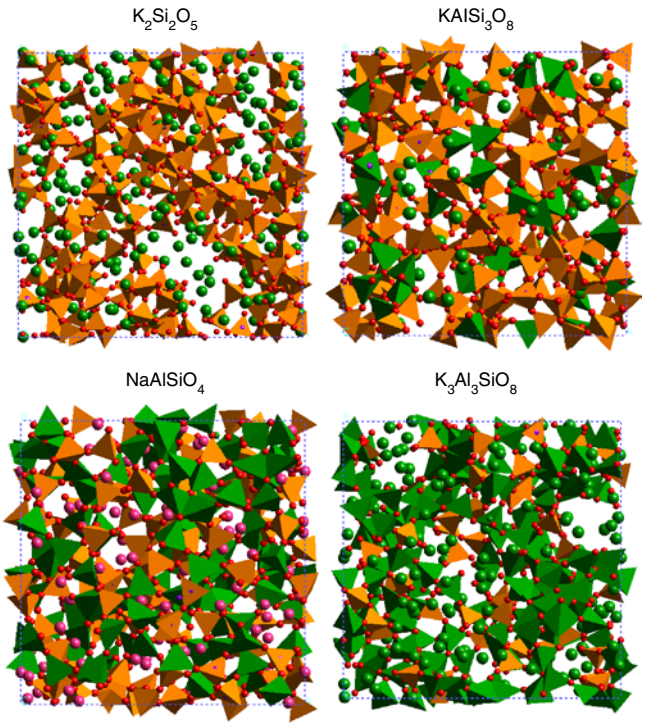

Figure 1. Example glass structures at 293 K.

cooling, the structures revert to mainly tetrahedral coordination of Al and Si, but some other polyhedra remain. Figure 2 shows the evolution of coordination polyhedra in the structures. The majority of the glass structures contain 100% tetrahedra, although a few fivefold- and sixfold-coordinated polyhedra around Al and Si persist in some structures. This becomes relevant when computing the vibrational properties, as is discussed below.

3.3. Radial distribution functions

The atomic RDF for each composition was determined using an in-house customization of Cerius[2]. The probability of finding an atom of type j within a spherical shell of radius r and thickness dr from atom i is given as $\rho_j g_{ij}(r) 4\pi r^2 \,\mathrm{d}r$, where ρ_j is the number of atoms of type j per unit volume, and $g_{ij}(r)$ is the atomic RDF. We form the functions

$$t_{ij}(r) = 4\pi r g_{ij}(r) = n_{ij}(r)/r \tag{5}$$

where the integral of $n_{ij}(r)$ gives the number of contacts within a given range of values of r. Sample plots of $t_{ij}(r)$ are given for $Na_2Si_2O_5$, $KAlSi_3O_8$ and $KAlSiO_4$ in figure 3. Also shown in these figures is the sum of the atomic pair correlation functions, $T(r)$.

The first peaks are Si–O, Al–O (if Al is present) and O–O. The RDFs for the disilicates show a broader and rather asymmetric Si–O peak than those for the other compounds, due to the presence of non-bridging oxygens (NBOs) in the disilicate structures—Si–O^{NBO} are distinctly shorter than Si–O^{BO}. For example, we chose at random ten bonds of each type in the $K_2Si_2O_5$ structure; the average Si–O^{NBO} length was 1.473 Å, while the average Si–O^{BO} length was 1.612 Å.

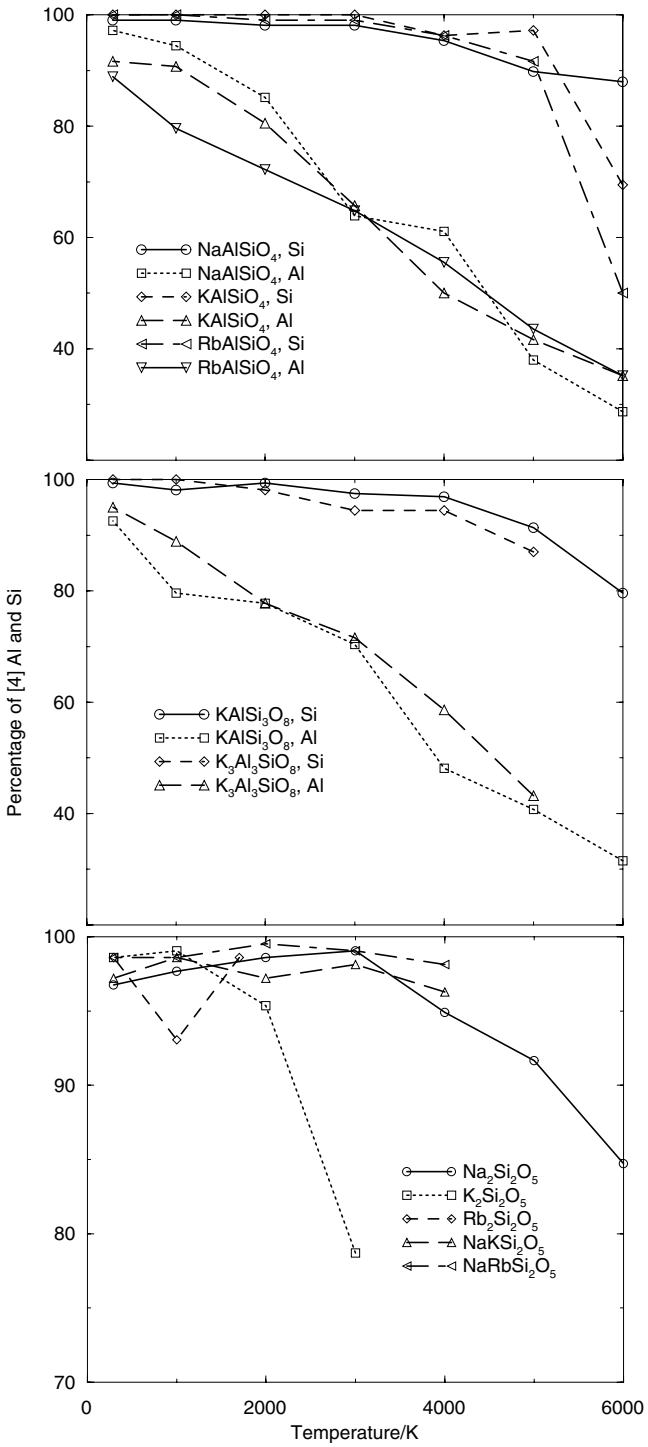

Figure 2. Percentage of tetrahedrally coordinated Si (and Al where applicable) in the glasses at each stage of MDS.

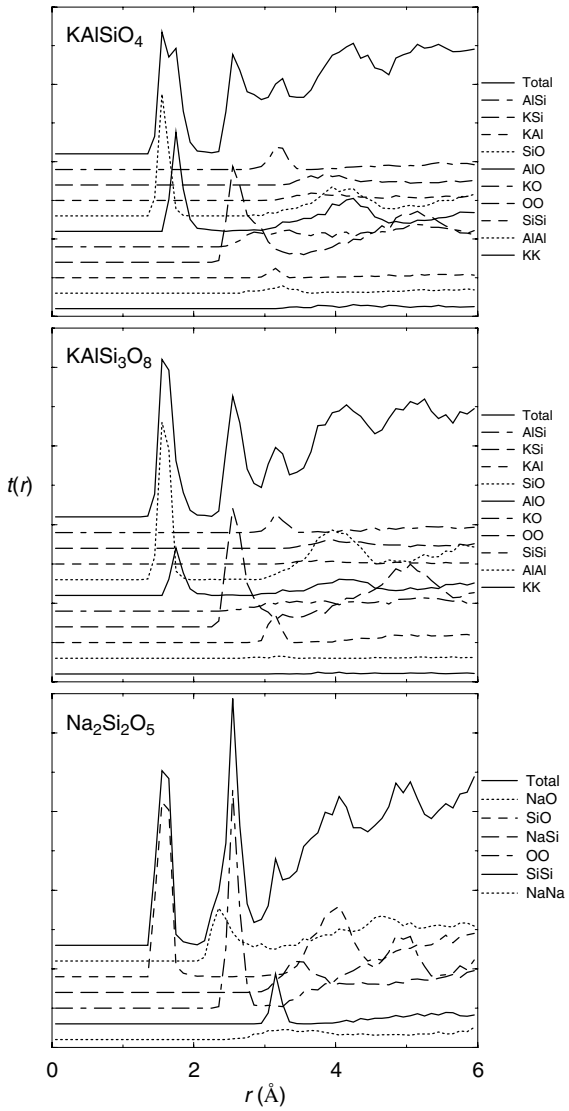

Figure 3. Calculated RDF for the glasses, in $T(r)$ form ('Total'), showing constituent $t_{ij}(r)$ functions.

3.4. Comparison of calculated RDFs with experiment

Experimentally determined RDFs exist for $Na_2Si_2O_5$ (x-ray diffraction) [19] and $KAlSi_3O_8$ (neutron diffraction) [20]. These are reproduced in $t(r)$ form in figure 4 for comparison with figure 3.

Our main interest here is to compare the positions of the main features with our calculated individual pair RDFs. The main features in the experimental RDF for K-feldspar are reproduced in our calculations. In the case of sodium disilicate, the O–O RDFs are not observed because the oxygen scattering power for x-rays is too weak. The remaining features are reproduced in our calculated pair RDFs.

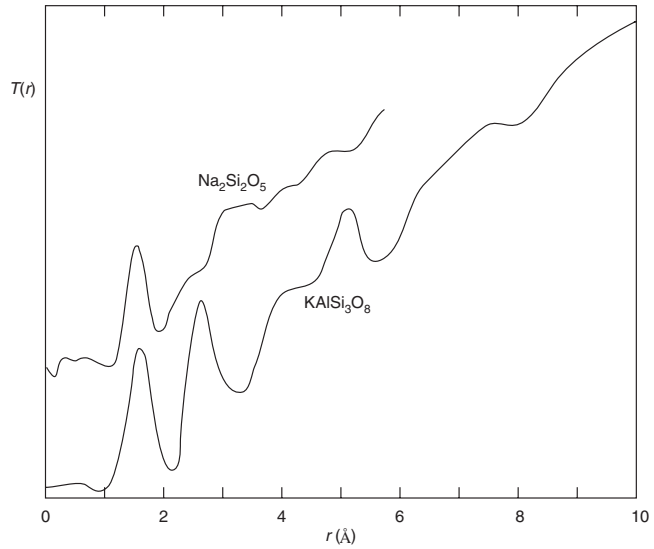

Figure 4. Experimentally determined RDFs for $Na_2Si_2O_5$ and $KAlSi_3O_8$. Reproduced from [19] and [20].

Table 2. Number densities (atoms $Å^{-3}$) for glasses. ρ indicates total number density; ρ' indicates number density of tetrahedral atoms (Si, Al if present, O).

Q^3			Q^4		
Glass	ρ	ρ'	Glass	ρ	ρ'
$Na_2Si_2O_5$	0.058	0.045	$NaAlSiO_4$	0.067	0.057
$NaKSi_2O_5$	0.052	0.040	$KAlSiO_4$	0.054	0.046
$NaRbSi_2O_5$	0.051	0.040	$RbAlSiO_4$	0.052	0.044
$K_2Si_2O_5$	0.044	0.035	$KAlSi_3O_8$	0.058	0.054
$Rb_2Si_2O_5$	0.043	0.034	$K_3Al_3SiO_8$	0.053	0.042

3.5. Number densities

The number densities (in atoms $Å^{-3}$) of the glasses are given in table 2, both for all atoms and for tetrahedral atoms alone. There is approximately 25% variation in number density for the Q^4 compounds and approximately 35% variation for the Q^3 compounds. Such a variation is of course expected, since larger cations will necessitate the formation of larger voids in the silicate framework, and will hence decrease the number density.

The number density is of interest because it may be an important factor in the RUM analysis. The lower the density, the more open the framework of linked tetrahedra, and the degree of openness may be expected to have an impact on the flexibility of the framework. Part of the motivation for this study is to examine this possibility, and is the reason why we have worked with samples that have a wide range of densities.

4. Analysis of MDS dynamics

In order to characterize the glasses, we analysed their structures in three ways. Firstly, we calculated the phonon density of states, $g(\omega)$, to examine vibrational similarities between

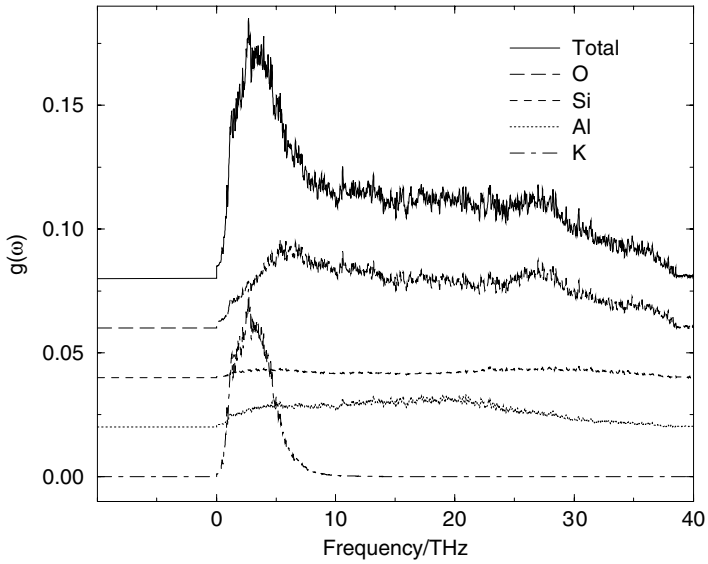

Figure 5. Phonon density of states for $K_3Al_3SiO_8$ showing contributions from each atom type. Scale is offset on x-axis for clarity.

glasses of the same compositional suites, and to determine the nature of contributions to $g(\omega)$ from each type of atom. Secondly, we investigated the large-scale flexibilities of the glasses by probing their ability to undergo structural reorientations. Finally, we investigated the short-term structural variations by comparing configurations at regular intervals during MDS and analysing the differences between them.

4.1. Phonon densities of states

For each glass, the trajectories of atoms were recorded during the MDS. These trajectories were then used to calculate the velocity autocorrelation function:

$$C(t) = \frac{\langle \boldsymbol{v}(0) \cdot \boldsymbol{v}(t) \rangle}{\langle |\boldsymbol{v}(0)|^2 \rangle} \tag{6}$$

with the angle brackets $\langle \cdots \rangle$ indicating an average over time and over all atoms. The Fourier transform of the mass-weighted velocity correlation function gives the phonon density of states, $g(\omega)$ [21]. Such calculations were performed for each glass, and two examples are given in figures 5 (for $K_3Al_3SiO_8$) and 6 (for $NaKSi_2O_5$). Also shown in these figures are the contributions from each atom type. The alkali cations contribute to the low-frequency vibrations and the tetrahedral atoms to the higher-frequency vibrations.

The total densities of states for compositional suites (disilicates, $XAlSiO_4$ and the $(KAlO_2)_x \cdot (SiO_2)_{1-x}$ series) are given in figure 7. These totals are shown without contributions from alkali cations, to enable easy comparison with those of amorphous silica [10] and crystalline α-cristobalite [22].

The glasses within each of the disilicate and $XAlSiO_4$ series are remarkably similar. Those in the $(KAlO_2)_x \cdot (SiO_2)_{1-x}$ series are slightly different at higher frequency, but this is not within the focus of this paper. The differences at low frequency between the amorphous and crystalline phases of silica are that the crystalline phase has a relatively slow rise with ω^2 due to the acoustic modes, with distinct peaks due to low-lying optic modes, whereas

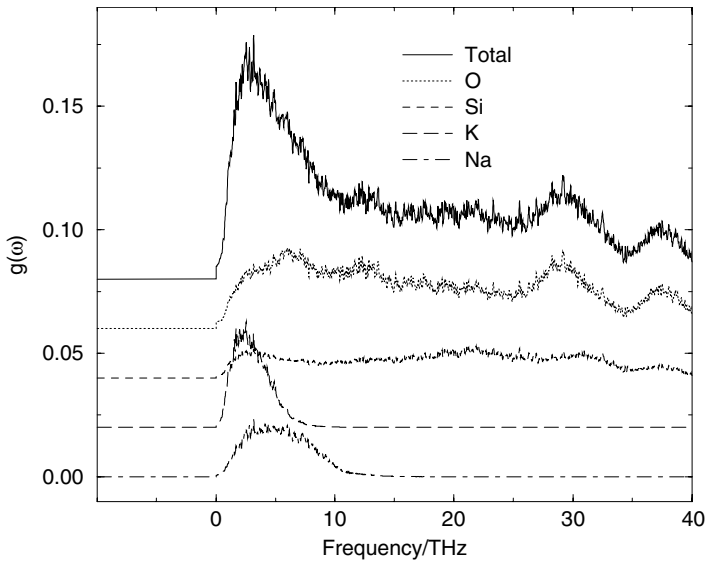

Figure 6. Phonon density of states for $NaKSi_2O_5$ showing contributions from each atom type. Scale is offset on x-axis for clarity.

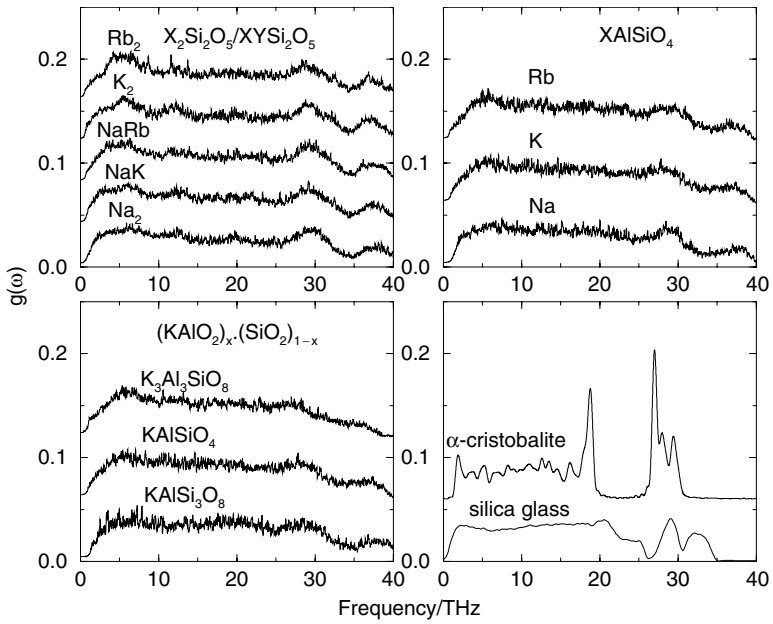

Figure 7. Total phonon density of states, excluding contributions from alkali cations, for all the glasses studied. Also shown for comparison are the densities of states of α-cristobalite (see [22]) and silica (calculation, [10]).

the density of states for silica glass rises somewhat faster without a clear distinction between acoustic and optic modes. The aluminosilicate glasses in this study all appear to lie between these two extremes. The rise at low frequency is not as fast as in silica glass, but clearly

the low-frequency optic modes are spread to the lowest frequencies. There is no systematic variation with density, although we shall point out some effects of density later in section 5. It is also interesting that the densities of states for the disilicates are not substantially different from those of the fully networked glasses; we shall comment on this later.

4.2. Large-scale structural reorientations

Glasses are known to exhibit anomalous thermal properties at low temperatures. For example, the variation of heat capacity with temperature scales approximately linearly, as opposed to the normal Debye result, $C \propto T^3$ (see, for example, [23]). One proposed explanation for this phenomenon is the existence of excess low-energy vibrational states [24]. Specifically, the model suggests the existence of localized low-energy excitations in glasses, with the atoms taking part in these vibrations being those for which the energy barrier is of the order of $k_B T$. The possibility of tunnelling between the minima of double-well potentials with such energy barriers is the main point of this model, hence leading to two-level tunnelling states.

However, the presence of double-well potentials in glasses has not been easy to identify. In a previous paper [2] it was noted that, during molecular dynamics simulation, parts of the structure of the silica glass model were able to undergo co-operative rearrangements. These rearrangements were identified as being responsible for two-level tunnelling states in [25] and [26].

We performed further MDS runs on $K_2Si_2O_5$, $K_3Al_3SiO_8$, $KAlSiO_4$, $RbAlSiO_4$ and $KAlSi_3O_8$, in order to look for evidence for these rearrangements. For each of these, we calculated σ, the mean square displacement of each atom:

$$\sigma = \langle |r|^2 \rangle - |\langle r \rangle|^2 \tag{7}$$

where r is the position of the atom. From this we formed the probability distribution function $P(\sigma)$ for each glass; examples are given in figure 8. Atoms with larger values of σ are likely candidates for participation in large jumps between two minima of double-well potentials. The majority of atoms with large σ values were found to be oxygen atoms, which is consistent with the involvement of motions of whole tetrahedra.

Analysis of $P(\sigma)$ plots for the glasses showed evidence for rearrangements in $KAlSiO_4$, $K_3Al_3SiO_8$ and $K_2Si_2O_5$. No atoms with large σ values were observed in $KAlSi_3O_8$ (as can be seen in figure 8) or $RbAlSiO_4$.

Figure 9 shows the positions of two large-σ oxygen atoms in $KAlSiO_4$ as a function of time. The atoms jump into a new position at ∼17 ps and back again to the old positions at ∼28 ps. Figure 10 shows a snapshot of the structure at 18.5 ps with the initial structure superimposed to illustrate the structural rearrangement, and also a snapshot at 30 ps to illustrate the rearrangement back to the initial configuration (again with the initial structure superimposed).

In $K_3Al_3SiO_8$, a rearrangement is seen at ∼28 ps. Here, the atoms do not jump again within the timescale of the simulation. A snapshot of the structure at 29 ps is given in figure 11.

In $K_2Si_2O_5$, several rearrangements were seen, all mainly involving one Q^1 SiO_4 tetrahedron. One of these occurred at ∼9.9 ps and is shown in figure 12. Note that a previous rearrangement has occurred and the jump is from this configuration back to the original configuration.

For the jump motions in question, we calculated the participation ratio

$$\mathcal{P}_{\text{jump}} = \frac{\left(\sum |\boldsymbol{u}_{\text{jump}}|^2\right)^2}{N \sum |\boldsymbol{u}_{\text{jump}}|^4} \tag{8}$$

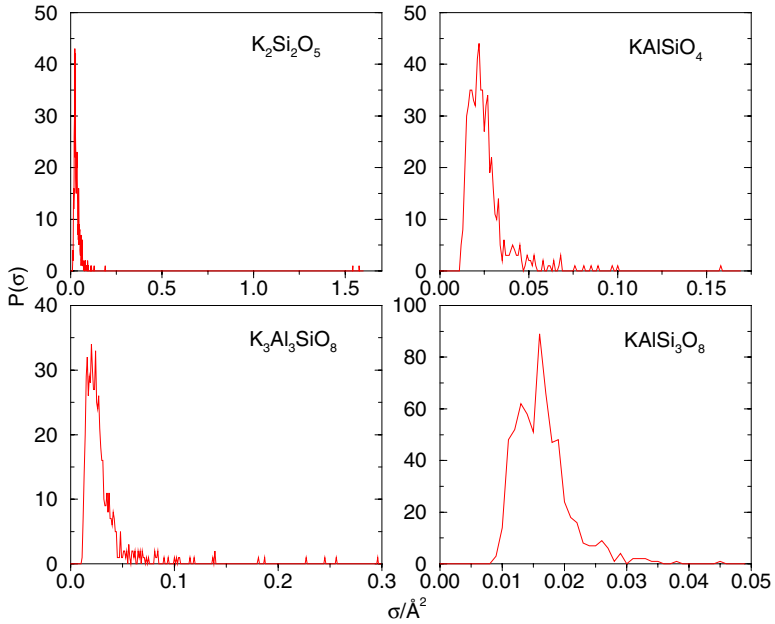

Figure 8. Plots of the distribution of atomic mean square displacements, $P(\sigma)$, for four glasses. Note the different scales on the x-axis, reflecting the highest σ values in each case.

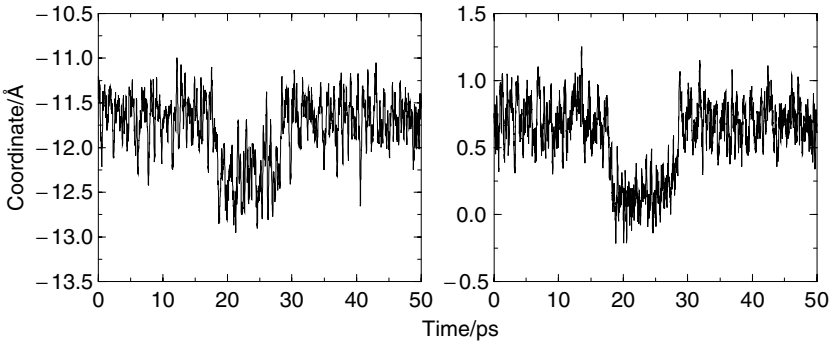

Figure 9. Coordinates of two oxygen atoms in $KAlSiO_4$, showing jump at ∼17 ps and back at ∼28 ps.

where $\boldsymbol{u}_{\text{jump}} = \boldsymbol{r}_{\text{after}} - \boldsymbol{r}_{\text{before}}$ is the difference between coordinates after and before the jump. Collective motions in which all atoms participate equally will have $\mathcal{P}_{\text{jump}} \sim 1$, but motion involving a single atom will have $\mathcal{P}_{\text{jump}} \sim 1/N$.

The jumps in figures 10–12 were found to have $N\mathcal{P}_{\text{jump}}$ values of 27 ($K_2Si_2O_5$), 91 and 105 (two jumps in $KAlSiO_4$) and 61 ($K_3Al_3SiO_8$). By comparison, the jumps observed in silica [2] had $N\mathcal{P}_{\text{jump}}$ values of around 30, although these were determined on structures at 50 K rather than 298 K.

Animations of the jumps represented in figures 10–12 are available in the online version of this article. They can also be viewed from http://www.esc.cam.ac.uk/movies/.

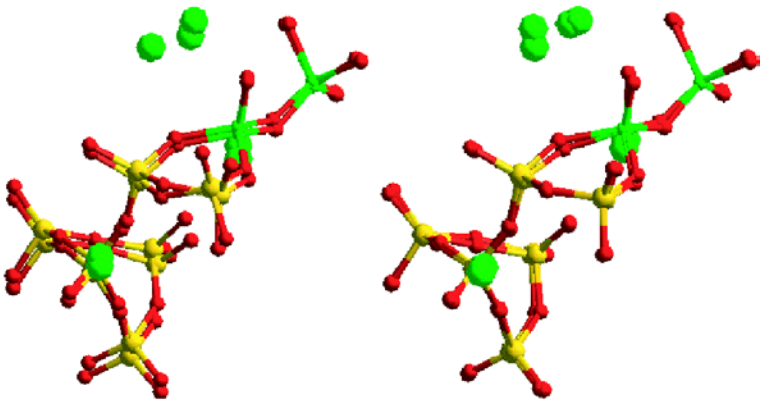

(a) t = 18.5ps after first jump.

(b) t = 30ps after second jump, back to original configuration.

Figure 10. Snapshots of a group of atoms in $KAlSiO_4$ at 18.5 and 30 ps, initial configuration superimposed. Oxygen atoms near the centre of the figure are those whose coordinates are given in figure 9. Animations of these jump events are available in the electronic version of the journal, file size 1 MB each.

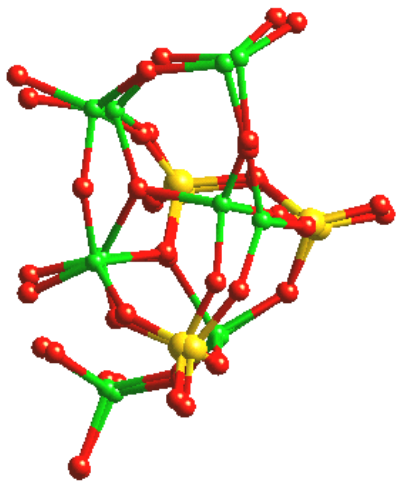

Figure 11. Snapshot of a group of atoms in $K_3Al_3SiO_8$ at 29 ps, initial configuration superimposed, showing rearrangement of the two atoms near the centre of the figure. An animation of this jump event is available in the electronic version of the journal, file size 1 MB.

4.3. Short-term structural variations

In addition to the analysis in section 4.2, which considers large-scale changes over comparatively large time periods, we can examine the flexibility of the glasses in an alternative way. For each glass, the final glass structure at 293 K produced from the simulation was used as the starting structure for a further simulation run, consisting of 2500 simulation steps and using the NVE ensemble (total simulation time 5 ps). The resulting output was then used as input for another 5 ps run, and this was repeated until four 5 ps runs were completed.

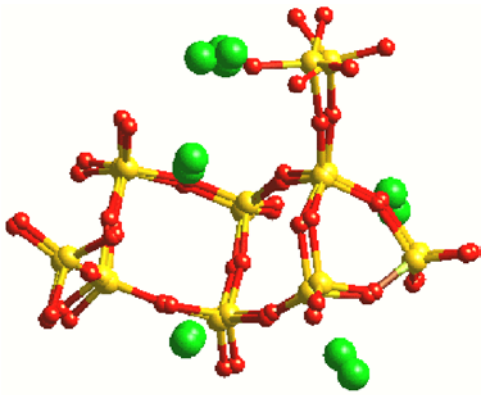

(a) t = 9.2ps before jump.

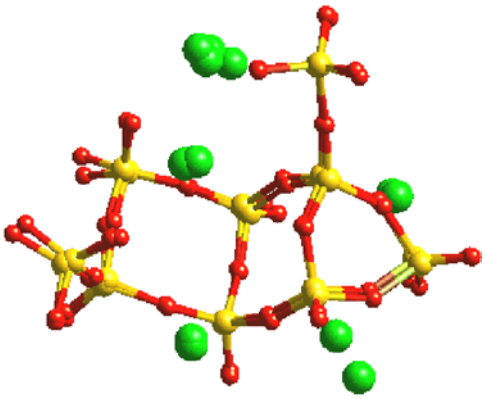

(b) t = 10ps after first jump.

Figure 12. Snapshots of a group of atoms in $K_2Si_2O_5$ at 9.2 and 10 ps, initial configuration superimposed. A previous rearrangement has occurred, and the jump is from this configuration back to the original configuration. Animations of these jump events are available in the electronic version of the journal, file size 2.9 MB each.

Each of the runs was compared with the previous one by calculating a general participation ratio:

$$\mathcal{P} = \frac{\left(\sum |\boldsymbol{u}|^2\right)^2}{N \sum |\boldsymbol{u}|^4} \tag{9}$$

where $\boldsymbol{u}$ refers to the displacement of an atom between snapshots, and the parameter N refers to the number of atoms in the structure. Large values of $\mathcal{P}$ imply that differences in structures between two configurations are spread across most atoms, whereas small values suggest that there are large localized differences between structures. These can occur if small groups of atoms can undergo large jump motions.

Participation ratios were calculated separately for the alkali cations in the structure and the tetrahedron-forming cations (Si, Al if present, O). Values of $\mathcal{P}$ near zero indicate localized short-term variation in the structure, and values nearer unity indicate that any short-term variation is co-operative across larger regions. The participation ratios calculated for the alkali metal cations in each glass are given in table 3, and those for the tetrahedron-forming cations are given in table 4.

Table 3. Participation ratios for alkali metal cations in the glasses.

		Values between snapshots at:			
Glass	Species	5 and 10 ps	10 and 15 ps	15 and 20 ps	Average
$Na_2Si_2O_5$	Na	0.178	0.241	0.296	0.238
$K_2Si_2O_5$	K	0.406	0.316	0.362	0.362
$Rb_2Si_2O_5$	Rb	0.268	0.400	0.310	0.326
$NaKSi_2O_5$	Na	0.268	0.344	0.278	0.296
	K	0.388	0.190	0.271	0.283
$NaRbSi_2O_5$	Na	0.500	0.363	0.441	0.435
	Rb	0.274	0.446	0.343	0.354
$NaAlSiO_4$	Na	0.337	0.301	0.427	0.355
$KAlSiO_4$	K	0.431	0.480	0.348	0.420
$RbAlSiO_4$	Rb	0.297	0.294	0.486	0.359
$KAlSi_3O_8$	K	0.459	0.388	0.274	0.374
$K_3Al_3SiO_8$	K	0.307	0.233	0.284	0.275

Table 4. Participation ratios for tetrahedron-forming atoms (Si, Al if present, O) in the glasses.

	Values between snapshots at:			
Glass	5 and 10 ps	10 and 15 ps	15 and 20 ps	Average
$Na_2Si_2O_5$	0.437	0.409	0.533	0.460
$K_2Si_2O_5$	0.432	0.424	0.329	0.395
$Rb_2Si_2O_5$	0.436	0.453	0.508	0.466
$NaKSi_2O_5$	0.420	0.431	0.496	0.449
$NaRbSi_2O_5$	0.462	0.533	0.519	0.503
$NaAlSiO_4$	0.525	0.514	0.488	0.509
$KAlSiO_4$	0.476	0.484	0.546	0.502
$RbAlSiO_4$	0.457	0.544	0.561	0.521
$KAlSi_3O_8$	0.495	0.533	0.535	0.521
$K_3Al_3SiO_8$	0.531	0.428	0.413	0.457

The values of the participation ratios for all systems are smaller for the alkali cations (average around $1/3$) than for the tetrahedral atoms (average closer to $1/2$). This is consistent with the fact that the tetrahedral atoms are linked into an infinite network, and therefore motions of the tetrahedral atoms will have higher correlations with neighbouring atoms. The motions of the alkali cations can only be correlated through their coupling to the network, and it is probable that some alkali cations have a weaker coupling than others. For the tetrahedral atoms, the disilicates have a slightly lower average participation number. This follows from the fact that there are significantly more non-bridging Si–O or Al–O bonds in the disilicates, leading to the possibility of large-amplitude localized motions of groups of tetrahedra that are not fully connected to the network.

5. RUM analysis

In crystalline silicates, it is often found that RUMs lie on special planes of wavevectors, which are determined by the crystal symmetry. Such planes of wavevectors are absent in glasses, and hence we need to use a different method for RUM analysis. This method involves calculating the density of states, as has been used to study the RUM flexibility of some crystalline

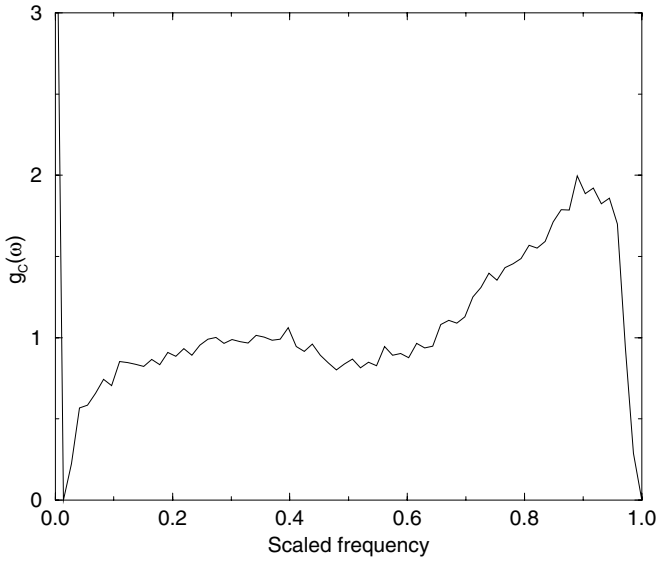

Figure 13. Hypothetical density of states for a silica glass configuration with 9% of the tetrahedra removed, for comparison with CRUSH densities of states for disilicates.

systems [5, 8]. The true RUMs will be calculated to have zero frequency, but modes on the same phonon branch as the RUMs with wavevectors close to the RUM wavevectors will have very low frequencies. The density of states approach will highlight the RUM flexibility through the calculation of the frequencies of these other modes. In a normal system without RUMs, the density of states will follow the normal Debye behaviour, i.e. $g(\omega) \propto \omega^2$. On the other hand, if a system contains RUMs, the limiting form of $g(\omega)$ will deviate from the Debye behaviour, often tending towards a constant value as $\omega \to 0$, or for particularly flexible networks having a peak in $g(\omega)$ around $\omega = 0$.

The program we used for the RUM analysis is CRUSH [27,28]. This program treats the SiO_4 and AlO_4 tetrahedra as rigid units within the framework of molecular lattice dynamics. All bridging oxygen atoms are replaced by pairs of atoms that are associated with one tetrahedron or the other, and these split atoms are held together by harmonic springs with equilibrium lengths of zero. The springs therefore act to resist any motion that moves them apart. Essentially the method involves solving the dynamical matrix for a random set of wavevectors and forming the density of states $g(\omega)$. We used random wavevectors to avoid artificial periodic effects in the density of states.

It should be noted that the density of states from CRUSH, which we shall label $g_C(\omega)$ for clarity, is not expected to resemble the density of states obtained from the MDS, $g(\omega)$; the latter is the more realistic quantity, but we are using CRUSH diagnostically as a method of quantifying the RUM flexibilities of the glasses. In the MDS the real forces will ensure that the RUMs do not have zero frequencies, so that the Debye limiting behaviour is observed for very small wavevectors. However, as was seen in the MDS calculations, the true density of states rises faster than the Debye form on increasing frequency.

The motivation for calculating $g_C(\omega)$ for the glasses studied in this work is to investigate whether the differing connectivities (Q^3 versus Q^4) of the glasses results in different low-frequency flexibility, and whether the results for silica glass with artificial defects from [2] are reproduced in real glasses with similar connectivities (i.e. the disilicates).

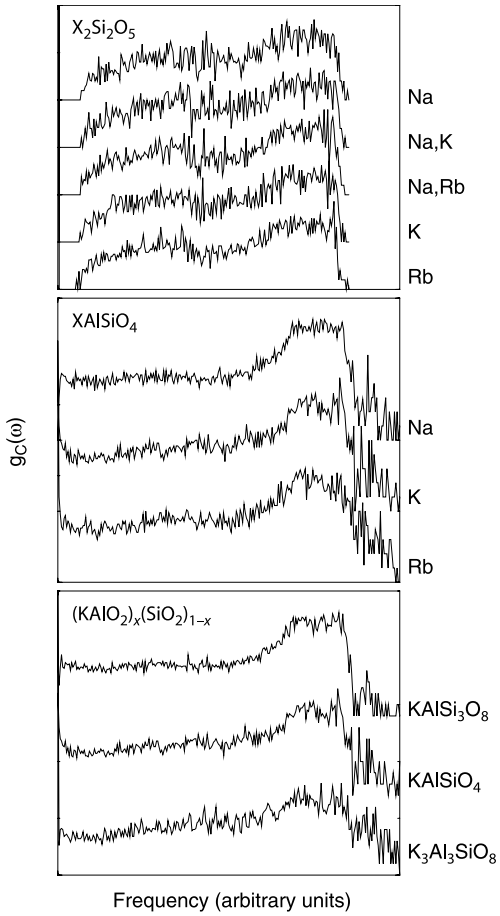

Figure 14. CRUSH densities of states. The large numbers of RUMs (up to 300) in the disilicates are not shown.

The $g_C(\omega)$ curve for defect silica glass in [2] is reproduced in figure 13. By comparison, the $g_C(\omega)$ for the glasses in this study are given in figure 14. The two main observations are (a) the similarity of the $g_C(\omega)$ for the disilicates with that of the defect silica glass and (b) the similarity between $g_C(\omega)$ for glasses in the same compositional suite.

The similarity between $g_C(\omega)$ for the defect silica glass and $g_C(\omega)$ for the disilicates is convincing, with both exhibiting a gap at $\omega \sim 0$ and a large number of RUMs compensating for this gap.

The similarity between CRUSH densities of states for glasses in the same compositional suite is somewhat surprising. We might expect that, since the number densities vary by up to 35%, the behaviour would also vary, but this is not the case.

We also note that the different connectivities of the glasses results in different low-frequency behaviour. The densities of states for the Q^3 glasses has a large gap at low ω, compensated by the large number of RUMs, whereas in the case of Q^4 glasses tend towards a constant value as $\omega \to 0$. Hence, the Q^3 glasses exhibit much more RUM flexibility than the Q^4 glasses.

As an aside, we can comment on the behaviour for the $XAlSiO_4$ compounds. There is an apparent difference in the behaviour between these compounds at $\omega \sim 0$, which is shown in

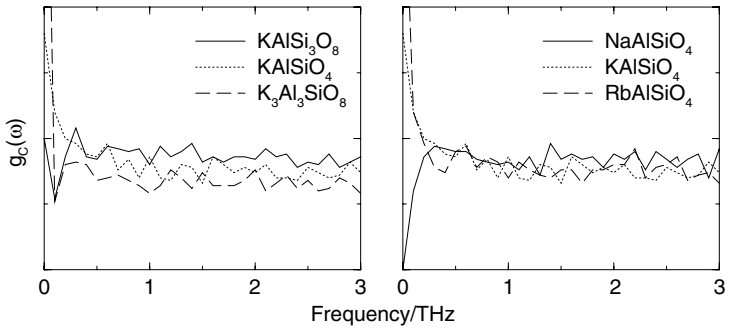

Figure 15. CRUSH densities of states for the $XAlSiO_4$ and $(KAlO_2)_x \cdot (SiO_2)_{1-x}$ compounds in the region $\omega \sim 0$. $KAlSiO_4$ is a member of both compositional series and hence appears on both plots.

figure 15—for X = K and X = Rb there are apparently higher numbers of RUMs than there are for X = Na. This is an artefact; the coordination polyhedron data for these compounds (figure 2) confirm this—there are a few non-tetrahedral polyhedra persisting in the equilibrium configurations at 293 K, thus there are a few non-bridging bonds, which have increased the apparent number of RUMs in the structures.

In addition to determining the number of RUMs present in the glasses, we can determine the extent to which they are localized. This is achieved by calculating the participation coefficient, $\mathcal{P}_C$:

$$\mathcal{P}_C = \frac{\left(\sum |u_C|^2\right)^2}{N \sum |u_C|^4}. \tag{10}$$

This equation is essentially similar to that for the participation ratio from section 4.2, but with the u_C being the atomic displacements associated with the CRUSH eigenvectors, and N being the number of units (in this case tetrahedra). $\mathcal{P}_C$ can take values from $1/N$ to 1 for a particular vibration, with a value of 1 indicating that all atoms participate equally in that vibration.

The participation coefficients for the glasses are given in figures 16–18. Also plotted for interest (see figure 19) are the participation coefficients for silica glass and the defect silica glass [10]. Some interesting points can be made; firstly, the $\omega = 0$ modes have the same spread of values (0–0.8) in the disilicates and the defect silica glass. However, the spread of $\mathcal{P}_C$ values for the other vibrations is approximately 0–0.8 for the disilicates, but only 0.4–0.8 for the defect silica glass—i.e. the vibrations in the real disilicates are more diverse in their degrees of localization than those in the defect silica glass.

Comparing the $\mathcal{P}_C$ plots for compositional suites, we note that once again, compounds within each of the disilicate and $XAlSiO_4$ suites behave similarly to one another. The spread of $\mathcal{P}_C$ values in the $XAlSiO_4$ series is much smaller than that in the disilicate series, suggesting as we might expect that the Q^4 network allows vibrations of a more co-operative nature, whilst the Q^3 networks allow vibrations which are rather more localized.

The $\mathcal{P}_C$ values for the $(KAlO_2)_x \cdot (SiO_2)_{1-x}$ series are rather interesting. All are ideally Q^4, and thus might be expected to have a small range of $\mathcal{P}_C$ values—but what actually happens is that as the potassium content increases, so does the spread of $\mathcal{P}_C$ values, suggesting that the alkali cations are also potentially responsible for changes in $\mathcal{P}_C$ trends between compounds in the series. It may be that this trend is due to alkali cations clustering together in the structures as their number increases—that is, vibrations in the tetrahedral network would be forced to be quite localized if regions of tetrahedra were separated by regions of alkali cations.

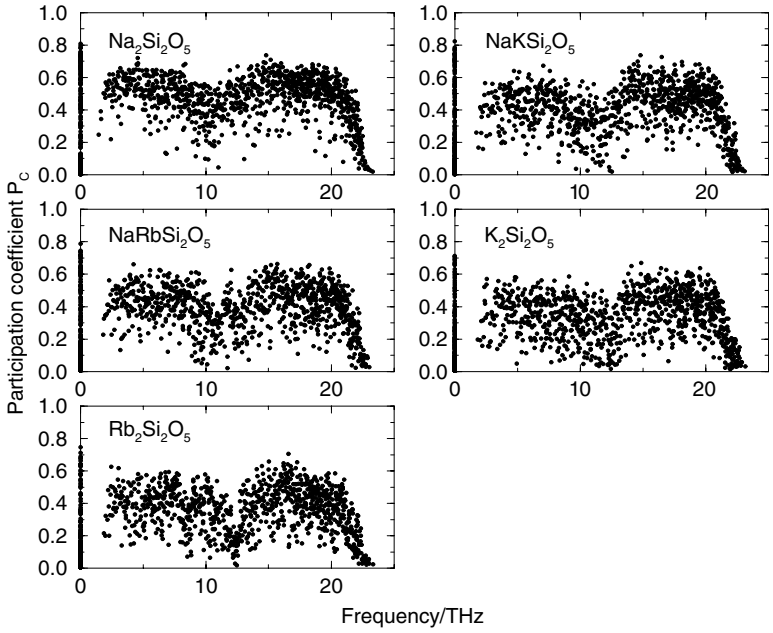

Figure 16. Participation coefficients from CRUSH for $X_2Si_2O_5$ and $XYSi_2O_5$.

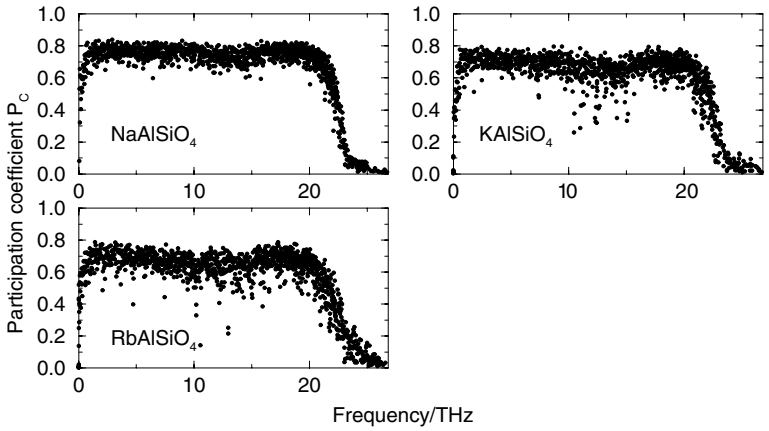

Figure 17. Participation coefficients from CRUSH for $XAlSiO_4$.

If we examine figure 20 we can see that the average participation coefficient for $K_2Si_2O_5$ is rather lower than one might expect from the other data (it is the point for which $\mathcal{P} = 0.29$). If one examines the structure of this glass from figure 1, it can be seen that there is a noticeable large, open region of K atoms visible just below the centre of the figure, and this cluster is somewhat larger than those in the Na analogue, and even slightly larger than those in the Rb analogue (structures not shown). This is an interesting point since it is one of the few apparent differences observed in this work between glasses of the same structural group. Similarly, examination of the $K_3Al_3SiO_8$ structure (figure 1) also shows two relatively large, open clusters of K atoms at the top left and top right, thereby supporting the suggested link

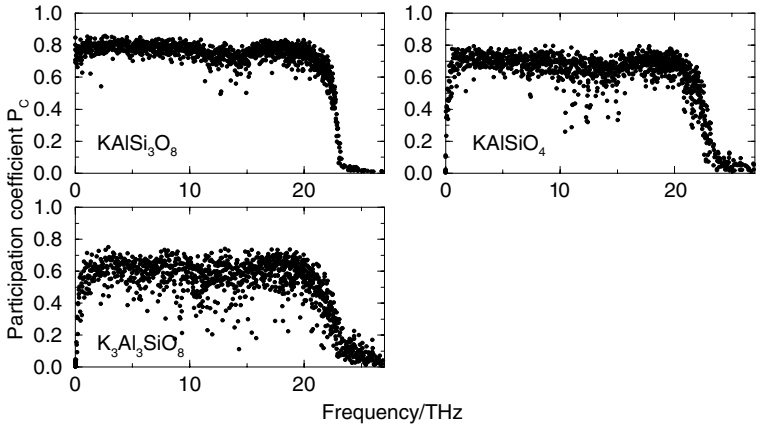

Figure 18. Participation coefficients from CRUSH for $(KAlO_2)_x \cdot (SiO_2)_{1-x}$.

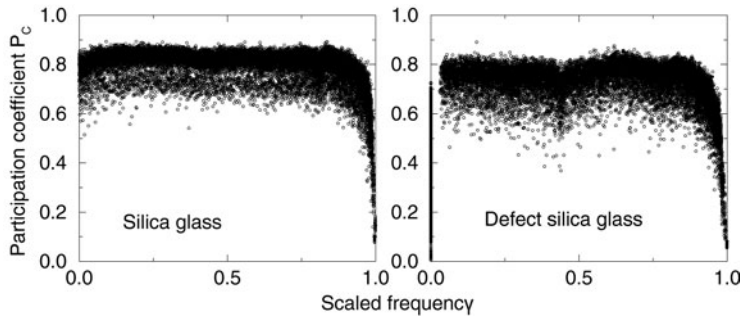

Figure 19. Participation coefficients from CRUSH for silica glass and defect silica glass. Reproduced from [10].

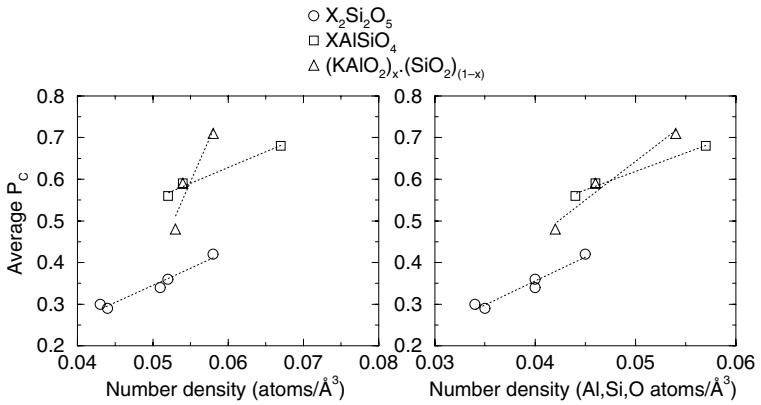

Figure 20. Plot of number density against average participation coefficients from CRUSH. Dotted lines are best fit lines for compositional series.

between alkali clustering and larger ranges of $\mathcal{P}_C$ values.

6. Conclusion

This work has focused on comparing the low-energy dynamics of silicate and aluminosilicate glasses with different number densities and different connectivities of tetrahedra. Changing number density has been achieved through the inclusion of network-modifying cations of different size, which causes the networks of linked SiO_4 and AlO_4 tetrahedra to form cavities of different sizes. The study has included disilicate and tectosilicate glasses to look for effects of significant numbers of NBO atoms. The two main tools have been MDS using realistic interatomic potentials, and the tools of the RUM model. Results have been compared with a recent study of silica glass.

The *first* main result is that the low-energy dynamics of the tectosilicate glasses are relatively insensitive to the number density. This is perhaps surprising, as it might be expected that more open structures would have a greater degree of flexibility. These similarities were seen in the densities of states obtained by MDS and through the calculations of the RUM spectra. The only significant effect of number density was in the participation ratios for RUM motions, where it was found that the more open structures (those with lower density) have a greater degree of localization of the vibrations. All tectosilicates studied here have a lower degree of low-energy flexibility than for silica glass, which is likely due to the additional binding effects of the network-modifying cations.

The *second* main result has been to confirm the prediction of the effects of non-bridging Si–O and Al–O bonds on the RUM spectra that was presented in the earlier study of silica glass. The existence of non-bridging bonds gives more flexibility to the network. It had been predicted that the existence of non-bridging bonds would give additional RUMs, which would be taken from the low-frequency distribution of frequencies rather than from across the broad distribution of mode frequencies. This result was clearly confirmed for all disilicates studied.

The *third* main result was the observation of large-amplitude reorientational motions of groups of tetrahedra similar to those observed in silica glass. These motions have been identified with the motions associated with two-level tunnelling states in silica glass, and it is useful to have found similar motions in other silicate glasses.

Acknowledgments

The DL_POLY simulations were performed on the Hitachi SR2201 parallel computer of the University of Cambridge's High Performance Computing Facility. EJP is grateful to Dr Mark Calleja for assistance with making the animations.

References

[1] Smith W and Forester T R 1996 DL_POLY_2.0: A general-purpose parallel molecular dynamics simulation package *J. Mol. Graph.* **14** 136–41

[2] Trachenko K O, Dove M T, Hammonds K D, Harris M J and Heine V 1998 Low energy dynamics and tunneling states in silica glass *Phys. Rev. Lett.* **81** 3431–4

[3] Harris M J, Dove M T and Parker J M 2000 Floppy modes and the boson peak in crystalline and amorphous silicates: an inelastic neutron scattering study *Mineral. Mag.* **64** 435–40

[4] Thorpe M F, Djordjevic B R and Jacobs D J 1997 The structure and mechanical properties of networks *Amorphous Insulators and Semiconductors (NATO ASI Series)* ed M F Thorpe and M I Mitkova (Dordrecht: Kluwer) p 289

[5] Hammonds K D, Dove M T, Giddy A P, Heine V and Winkler B 1996 Rigid-unit phonon modes and structural phase transitions in framework silicates *Am. Mineral.* **81** 1057–79

[6] Pryde A K A, Dove M T and Heine V 1998 Simulation studies of ZrW_2O_8 at high pressure *J. Phys.: Condens. Matter* **10** 8417–28

[7] Heine V, Welche P R L and Dove M T 1999 Geometrical origin and theory of negative thermal expansion in framework structures *J. Am. Ceram. Soc.* **82** 1793–802
[8] Dove M T, Trachenko K O, Tucker M G and Keen D A 2000 Rigid unit modes in framework structures: theory, experiment and applications *Rev. Mineral. Geochem.* **39** 1–33
[9] Swainson I P and Dove M T 1993 First-principles studies on structural properties of β-cristobalite *Phys. Rev. Lett.* **71** 3610
[10] Trachenko K O, Dove M T, Harris M J and Heine V 2000 Dynamics of silica glass: two-level tunnelling states and low-energy floppy modes *J. Phys.: Condens. Matter* **12** 8041–64
[11] Dove M T, Hammonds K D, Harris M J, Heine V, Keen D A, Pryde A K A, Trachenko K O and Warren M C 2000 Amorphous silica from the rigid unit mode approach *Mineral. Mag.* **64** 377–88
[12] Huang C and Cormack A N 1991 Structure and energetics in mixed-alkali-metal silicate glasses from molecular dynamics *J. Mater. Chem.* **2** 281–7
[13] Gale J D 1997 GULP—a computer program for the symmetry adapted simulation of solids *J. Chem. Soc.—Faraday Trans.* **93** 629–37
[14] Gruenhut S, Amini M, MacFarlane D R and Meakin P 1997 Molecular dynamics glass simulation and equilibration techniques *Mol. Simul.* **19** 139–60
[15] Garofalini S H 2001 Molecular dynamics simulations of silicate glasses and glass surfaces *Rev. Mineral. Geochem.* **42** 131–68
[16] Woodley S M, Battle P D, Gale J D and Catlow C R A 1999 The prediction of inorganic crystal structures using a genetic algorithm and energy minimisation *Phys. Chem. Chem. Phys.* **1** 2535–42
[17] Collins D R and Catlow C R A 1992 Computer simulation of structures and cohesive properties of micas *Am. Mineral.* **77** 1172–81
[18] Shelby J E 1997 Introduction to glass science and technology *R. Soc. Chem.*
[19] Imaoka M, Hasegawa H and Yasui I 1983 X-ray diffraction study of the structure of silicate glasses: II. Alkali disilicate glasses *Phys. Chem. Glasses* **24** 72–8
[20] Zotov N, Boysen H, Romano C, Dingwell D and Yanev Y 1995 Neutron diffraction study of feldspar glasses—mixed alkali effect *J. Non-Cryst. Solids* **191** 124–31
[21] Dove M T 1993 *Introduction to Lattice Dynamics* (Cambridge: Cambridge University Press)
[22] Swainson I P and Dove M T 1995 Molecular dynamics simulation of α- and β-cristobalite *J. Phys.: Condens. Matter* **7** 1771–88
[23] Tripodo G, D'Angelo G, Carini G, Bartolotta A, Fontana A and Rossi F 1999 Low energy vibrational dynamics and connectivity in borate glasses *J. Phys.: Condens. Matter* **11** A229–35
[24] Zeller R C and Pohl R O 1971 Thermal conductivity and specific heat of noncrystalline solids *Phys. Rev.* B **4** 2029–41
[25] Anderson P W, Halperin B I and Varma C M 1972 Anomalous low temperature thermal properties of glasses and spin glasses *Phil. Mag.* **25** 1–9
[26] Phillips W A 1972 Tunnelling states in amorphous solids. *J. Low Temp. Phys.* **7** 351–60
[27] Hammonds K D, Dove M T, Giddy A P and Heine V 1994 `CRUSH`—a FORTRAN program for the analysis of rigid-unit mode spectrum of a framework structure *Am. Mineral.* **79** 1207–9
[28] Dove M T `CRUSH`: The 'rigid unit mode' program. http://www.esc.cam.ac.uk/mineral_sciences/crush/